JOURNAL OF APPLIED ELECTROCHEMISTRY 17 (1987) 174–184

The impedance of alkaline manganese cells and their relationship to cell performance. II. Correlation with short-circuit current and initial pulse discharge behaviour

R. BARNARD, L. M. BAUGH*, C. F. RANDELL

Every Ready Limited, Technical Division, Tanfield Lea, Stanley, Co. Durham, UK

Received 11 March 1986

The theory relating the short-circuit or flash current behaviour of alkaline manganese and Leclanché cells to their internal resistance values has been reviewed. It is shown that the relationship SCC = VOC/R_i pertains for both cell types where SCC is the short-circuit current, VOC the voltage at open circuit and R_i the internal cell resistance which is a composite of several components. In the case of alkaline manganese cells these can be independently resolved using *in situ* impedance measurements into three major components: the electrolyte resistance within the anode–separator–cathode porous matrices; the resistance of the cathode (MnO_2 + graphite mixture); and the resistance of the nickel oxide layer on the surface of the nickel-plated steel positive current collector (cell container). In the case of Leclanché cells three components also control the internal resistance, but these cannot be so easily resolved. They are: the electrolyte resistance within the cathode separator matrices; the resistance of the cathode (MnO_2 + carbon); and contact resistance between the cathode and positive current collector (carbon rod). Equivalent circuits for both alkaline manganese and Leclanché cells are proposed.

Galvanostatic 2-A pulse discharge measurements have been made on LR20 alkaline manganese cells and directly correlated with the impedance measurements, thus providing confirmatory evidence for the equivalent circuit proposed. It is shown that the resistance calculated from the potential drop at 10 ms correlates closely with the internal resistance and hence short-circuit current value. It is also shown that ohmic polarization at long times (10 s) constitutes 67% of the total potential loss within the cell. Hence for a typical repetitive 2 A/10 s pulse discharge regime, the discharge life is critically dependent on the cell internal resistance value.

1. Introduction

In the previous paper [1] a detailed appraisal was made of the factors which determine the impedance characteristics of undischarged alkaline manganese cells. It was demonstrated that in the case of standard cells the impedance is dominated by that of the cathode–can assembly, the anode–separator impedance being negligible by comparison. It was also shown that the former impedance can be further resolved into two components. Firstly, that due to the nickel oxide layer on the surface of the nickel plated steel can, and secondly, that due to the cathode itself (manganese dioxide + graphite mixture). It was predicted from this work that these impedance characteristics would have significant consequences in regard to the discharge performance of the cells, particularly at high rates.

The simplest and most stringent high-rate discharge test which can be applied to a cell is to short its terminals and determine the instantaneous (maximum) current flow using a low-impedance, series-connected ammeter. The current measured under these conditions is called the flash or short-circuit current (SCC). This test

* *Present address*: BNF Metals Technology Centre, Grove Laboratories, Denchworth Road, Wantage, Oxon, UK.

0021–891X/87 $03.00 + .12

is applied extensively as a measure of quality and plays an important role in fault diagnosis. It has been demonstrated in the case of Leclanché cells [2, 3] that in the simplest analysis the SCC is directly proportional to the open-circuit voltage of the cell (VOC) and inversely proportional to its internal resistance, R_i. Thus

$$\text{SCC} = \text{VOC}/R_i \quad (1)$$

where Equation 1 is essentially a statement of Ohm's law. It can be seen from Equation 1 that the SCC responds primarily to changes in R_i, since for any particular cell chemistry the VOC is approximately constant, being determined predominantly by thermodynamic considerations only. The internal resistance can be determined by a variety of methods and these have been reviewed by Hamer [3]. The values which correlate most closely to those predicted by Equation 1 are determined by high-frequency impedance techniques or short-time pulse methods. At these frequencies (or time scales) the impedance becomes purely ohmic. While Equation 1 can now be regarded as satisfactory for Leclanché cells, it is still not clear which components within the cell are the major contributors to the internal resistance. Furthermore, to the knowledge of the authors, the application of the above general principles to other cell types does not appear to have been explored.

A second important high-rate test is to galvanostatically discharge the cell for a short time at a current which is somewhat less than the short-circuit value, but nevertheless appreciable, and determine the change in closed circuit voltage (VCC) with time. A typical test is 2 A for 10 s. The VCC falls continuously during the test, the extent of the drop in voltage (VOC − VCC) providing an inverse measure of the cell efficiency.

The present paper is concerned with an investigation aimed at correlating the initial impedance characteristics of alkaline manganese cells with their initial high-rate transient discharge behaviour. The correlation with both short-circuit current and initial galvanostatic pulse discharge behaviour has been examined. In the case of the former, results are also presented in respect of Leclanché cells and these are compared and contrasted with those for the alkaline manganese equivalent. This study was considered to be a necessary first step in providing the underlying theory required to understand the factors determining the longer term pulse discharge capacity. A consideration of the latter will be given in a subsequent communication.

2. Theoretical considerations

The relationship between the short-circuit current, open-circuit voltage and cell internal resistance can be derived as follows. Let the resistance of the series ammeter and its leads together with any contact resistances between the leads and the cell terminals be R_A. Then

$$R_A = \text{VCC}/\text{SCC} \quad (2)$$

Also,

$$(R_p)_{t\to 0} = R_i = \Delta V/\text{SCC} = (\text{VOC} - \text{VCC})/\text{SCC} \quad (3)$$

where R_p is the cell polarization resistance and ΔV is the near instantaneous change in cell voltage in the short-circuit measurement. Equation 3 applies because the contribution to the total polarization resistance from charge transfer and mass transfer effects at the electrodes is considered to be negligible at $t \to 0$. Therefore, from Equations 2 and 3:

$$R_i = (\text{VOC}/\text{SCC}) - R_A \quad (4)$$

Furthermore, if R_A is negligible compared with R_i then Equation 4 simplifies to

$$R_i = \text{VOC}/\text{SCC} \quad (5)$$

Experience shows that during SCC measurements on R20 Leclanché cells, for example, VCC $\approx$ 70 mV (at maximum current). Thus from Equation 2 for a 6 A SCC:

$$R_A \approx 70\,\text{mV}/6\,\text{A} = 11.7\,\text{m}\Omega$$

This value for the resistance of the ammeter, leads and cell contacts is small compared with the minimum R_i value of $\sim 0.20\,\Omega$, and at larger internal resistance values it becomes negligible.

In order to test Equation 5 for any particular cell chemistry, size or design, it is necessary to obtain the pertinent internal resistance value. This is best obtained from the cell impedance

spectrum at high frequencies. However, the internal resistance cannot be obtained unless a complete interpretation of the complex plane impedance behaviour is available because the extracted value must contain all the relevant resistive components. The following contributions must be included.

(i) Electrolyte resistance, R_e.

(ii) Contact resistance between the particles which constitute the electrode materials, e.g. MnO_2, zinc, carbon, etc., and resistance within the particles themselves, R_{part}.

(iii) Contact resistance at the interfaces between the current collectors and the electrode materials, R_1.

(iv) Resistance due to any additional phases present on the surfaces of the current collectors, e.g. oxides, R_{phase}.

(v) Contact resistance at the interfaces between the surface phases and the current collectors, R_2.

(vi) Resistance due to the current collectors themselves, R_{cc}.

The total internal resistance can then be defined as

$$R_i = R_e + R_{part} + R_1 + R_{phase} + R_2 + R_{cc} \quad (6)$$

where the parameters refer to the sum of both anode and cathode contributions, e.g. ($R_{part}^{an} + R_{part}^{cath}$), etc.

Clearly, the relative contributions from the above components to the total internal resistance of the cell will vary considerably with cell chemistry, size, design, geometry and quality of construction, etc. Furthermore, in most instances many of the contributions in Equation 6 will be negligible, resulting in a situation where perhaps only two or three components determine R_i. This will not be the case with faulty cells, however.

3. Experimental details

SCC measurements were made with a low impedance ammeter, Ernest Turner Ltd, type 509–86. The method of making the impedance measurements on individual cell components *in situ* has been discussed previously together with a description of the reference electrode probes [1]. Voltage–time transients were recorded on a Telequipment storage oscilliscope and were photographed on polaroid film. A Hi Tek wave form generator was used in conjunction with a Type TR40/3 A potentiostat to generate galvanostatically controlled 2-A pulses of either 10 ms or 4 s duration.

4. Results and discussion

4.1. *Correlation of impedance with short-circuit/flash current for Leclanché and alkaline manganese cells*

Fig. 1 compares and contrasts the complex plane impedance characteristics for an R20 Leclanché cell (Fig. 1a) with those for an LR20 alkaline manganese cell (Fig. 1b). It is clear that the shapes of these diagrams have little in common. Furthermore, the resistance–reactance scale on the impedance spectrum for the Leclanché cell is 25 times greater than that for the alkaline manganese equivalent. In fact, the entire spectrum for the latter fits into the space between the high frequency intercept and the origin of the former. These results partly explain the higher rate capability of alkaline manganese cells.

A detailed consideration of the factors which determine the overall impedance spectrum for Leclanché cells has been reported previously [4]. In agreement with the conclusion of Karunathilaka *et al.* [5] the impedance characteristics can be attributed exclusively to the anode. The large semicircle of diameter 7.5 Ω can be ascribed to a charge-transfer resistance for the zinc exchange reaction in parallel with a double layer capacity for the zinc–electrolyte interface. As a result of this the internal resistance can simply be determined from the infinite frequency extrapolation of the impedance spectrum. In the case of Leclanché cells where the anode cup is also the anode current collector (cell container), simplification of Equation 6 is possible since R_{phase} and R_2 are absent and R_{cc} can be assumed negligible. Hence

$$R_i = R_e + R_{part}^{cath} + R_1^{cath} \quad (7)$$

where R_e refers to the resistance of electrolyte within the separator and cathode matrices; R_{part}^{cath} refers to the particle–particle contact resistance and inherent particle resistance; and R_1^{cath} refers to contact resistance between the cathode and

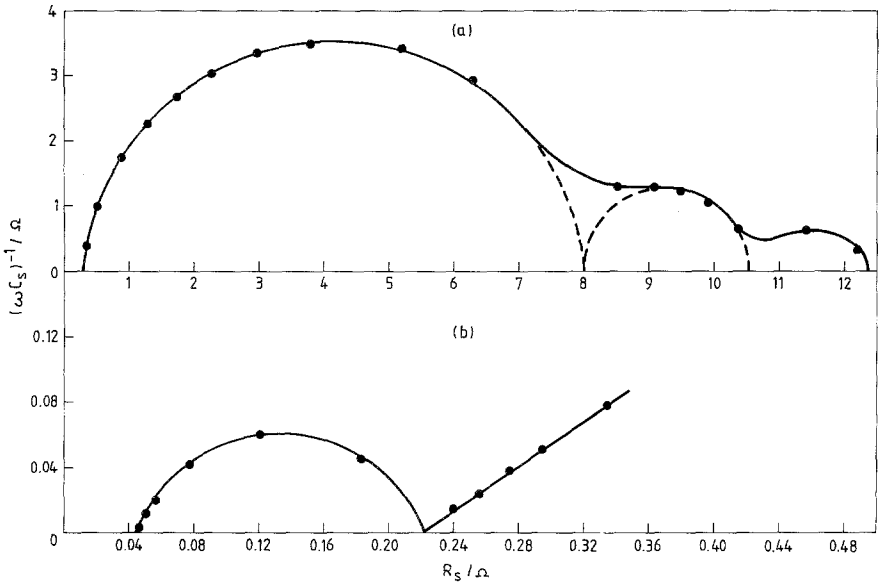

Fig. 1. Impedance spectra for undischarged cells in the frequency range 100 kHz to 1 mHz. (a) R20 Leclanché cell; (b) LR20 alkaline manganese cell.

the carbon rod positive current collector. Fig. 2 shows the test of Equation 5 for various R20 Leclanché cells using R_i values taken directly from the *high* frequency intercepts on the respective impedance diagrams as indicated schematically (inset). The tested cells differed widely in age, construction and exact formulation. Nevertheless, when the VOC range is taken into account it is clear that the predicted relationship is observed. The adherence of the data to Equation 5 confirms that the contact resistance at the battery terminals was minimal during both the SCC and impedance measurements.

The factors determining the overall impedance spectrum for alkaline manganese cells are more numerous than for Leclanché cells [1]. The high frequency intercept can be ascribed predominantly to electrolyte resistance within the cathode–separator–anode matrices. The semicircle is attributed to a combination of two factors, each of which may predominate according to the particular cell formulation considered. Firstly, at high frequencies, a contribution from the cathode and secondly, at lower frequencies, a contribution from the nickel oxide layer present on the surface of the nickel-plated steel positive current collector (cell container). Both components give rise to a semicircle in the complex plane, but their combination produces an 'envelope' or 'flattened' semicircle. When the nickel oxide is thick, as was the case for the cell whose impedance is shown in Fig. 1b, its resistance and reactance largely control the impedance characteristics and a single large semicircle is obtained. At very low frequencies a Warburg impedance emerges due to slow diffusion processes within the manganese dioxide, but this has no bearing on the present discussion since it is concerned with concentration polarization only. From the above discussion the internal resistance may be defined for alkaline manganese cells as

$$R_i = R_e + R^{cath}_{part} + R^{cath}_1 + R^{cath}_{phase} + R^{cath}_2 \quad (8)$$

or

$$R_i = R_e + R^{cath} \quad (9)$$

This is equivalent to the resistance of electrolyte + cathode–can assembly. Fig. 3 shows the test of Equation 5 for various LR20 alkaline manganese cells using R_i values taken directly from the low frequency intercept of the semicircle on the resistance axis as shown schematically (inset). All the tested cells had a VOC of

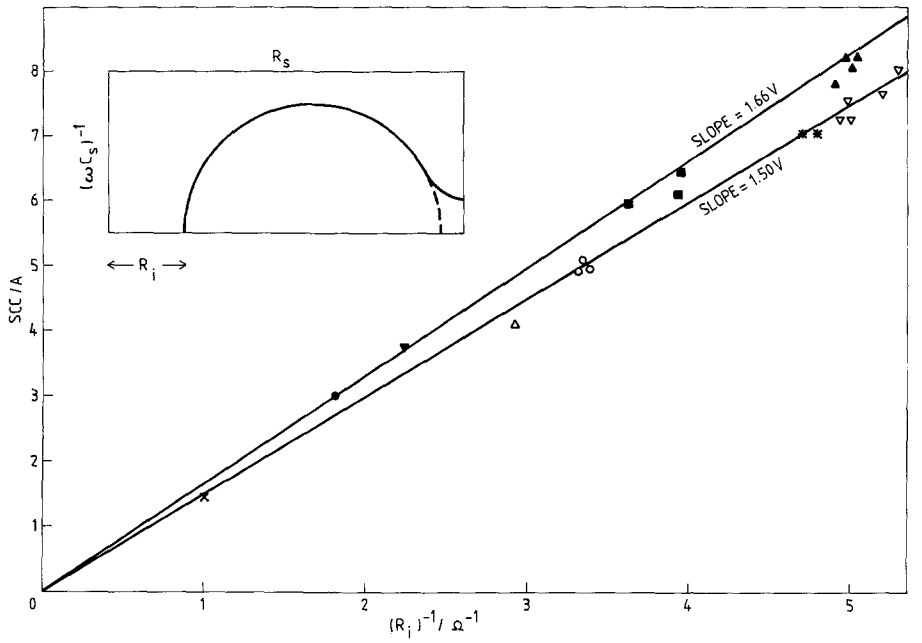

Fig. 2. Relationship between short-circuit current and internal resistance for Leclanché cells. (a) Plot of short-circuit current versus reciprocal internal resistance for various R20 size cells where like symbols indicate cells within a single batch. (b) Schematic diagram indicating the method of determining the internal resistance from the overall impedance spectrum.

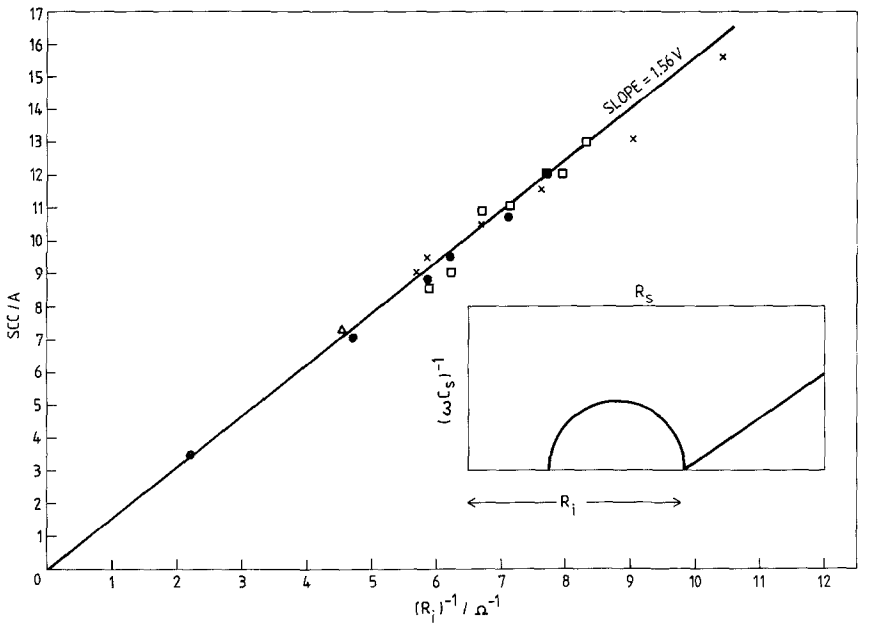

Fig. 3. Relationship between short-circuit current and internal resistance for alkaline manganese cells. (a) Plot of short-circuit current versus reciprocal internal resistance for various LR20 cells where like symbols indicate cells within a single batch. (b) Schematic diagram indicating the method of determining the internal resistance from the overall impedance spectrum.

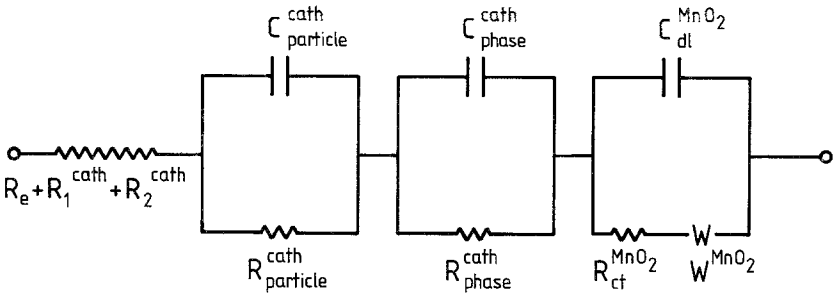

Fig. 4. Equivalent circuit for an alkaline manganese cell. The circuit is written such that the resistive component in the series R–C network diminishes progressively from right to left as the frequency increases. W, Warburg impedance; C_{part}, capacitance attributable to the cathode; C_{phase}, capacitance due to any phases present on the surface of the current collectors; C_{dl}, double-layer capacity.

1.56 V, but again differed widely in exact formulation. However, the expected relationship between SCC and R_i is obeyed accurately with little scatter except for the smallest R_i values ($< 0.11\,\Omega$) where evidence of contact resistance errors is just discernible.

The correlations given in Figs 2 and 3 provide important evidence which allows the equivalent electrical circuit for Leclanché and alkaline manganese cells to be represented with a reasonable degree of accuracy. In particular, the more complex circuit for the latter can be specified with greater confidence. In the previous paper [1] it was shown that two semicircles were discernible in the complex plane impedance diagram, one due to the oxide layer on the nickel plated steel can and one due to the cathode itself. It was considered unlikely that the cathode semicircle could be equated with a charge-transfer resistance due to the MnO_2 reaction in parallel with a double-layer capacity, although this was not proved. Fig. 3, however, confirms the correctness of this conclusion. The direct correlation of the SCC with the indicated R_i value could not have been obtained if the latter contained a component due to charge transfer. Thus in order to write the equivalent circuit, three series R–C networks must be included as shown in Fig. 4, the SCC responding to the circuit on the left hand side including the first two R–C networks only. The data presented [1] suggest that the charge-transfer resistance, R_{ct}, is very small compared with the other resistance values which therefore dominate. This conclusion is in general agreement with the results of Atlung and Jacobsen [6]. Nevertheless, R_{ct} is included for completeness. It should also be noted that a transmission line model can be used to represent the first and third R–C networks in Fig. 4. The complexity of the equivalent circuit for alkaline manganese cells contrasts with that for Leclanché cells which is relatively simple as shown in Fig. 5. As stated earlier, the SCC responds to the composite resistance on the left hand side of Fig. 5 only.

4.2. *Correlation of impedance with pulse discharge behaviour*

The short-circuit current data for alkaline manganese cells correlates directly with the resistive components of the left hand side of the equivalent circuit in Fig. 4, including those in the first two R–C networks. However, in the case of pulse discharge behaviour the extent to which

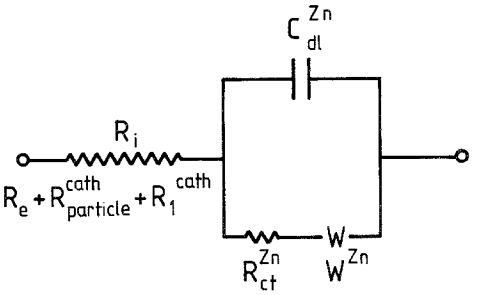

Fig. 5. Equivalent circuit for a Leclanché cell. The circuit is written such that the resistive component in the series R–C network diminishes progressively from right to left as the frequency increases. For definitions of resistive and capacitive components see text and Fig. 4.

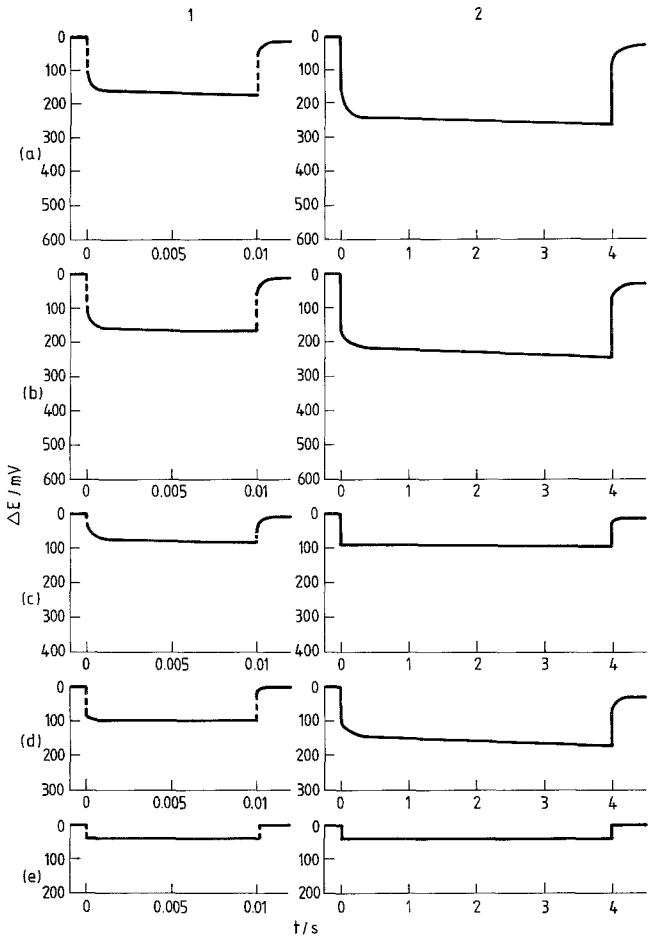

Fig. 6. Galvanostatic 2-A pulse discharge characteristic taken over 10 ms (column 1) and 4 s (column 2) for various components in a standard LR20 alkaline manganese cell. (a) Voltage response of the complete cell; (b) voltage response of the cathode–can assembly; (c) voltage response of the can; (d) voltage response of the anode–separator system + cathode; (e) voltage response of the anode–separator system.

similar correlations can be made will depend upon the time scale employed in the pulse measurements. Clearly, at long times the third R–C component in the equivalent circuit participates. Experiments were conducted to explore the relationship further.

A breakdown of the impedance characteristics for a standard LR20 alkaline manganese cell is shown in Fig. 2 of Part I of this work [1]; Fig. 2a is the impedance spectrum for the complete cell and Fig. 2b–e the impedance contributions from the individual cell components obtained using a reference electrode in two different positions. The interpretation of these impedance spectra together with the technique of measurement has been discussed in detail previously [1].

Fig. 6 shows the equivalent galvanostatic 2-A pulse discharge characteristics over two time intervals, 10 ms and 4 s. Fig. 6a shows the pulse discharge curve for the complete cell and Fig. 6b–e shows the pulse behaviour for the individual cell components obtained with the reference electrode in identical positions to those in Fig. 2b–e of Part I [1], respectively. Three regions of the voltage response in Fig. $6a_1$ can be identified at short times (10 ms pulse). Firstly, an instantaneous drop shown by the dotted line of magnitude 100 mV; secondly, a curved shoulder of magnitude ~ 50 mV; and finally a long tail increasing continuously with time until the end of the pulse. Using the longer 4-s pulse the results are superficially similar although quantitatively different. Thus the initial voltage drop in Fig. $6a_2$ is larger at 150 mV and there is a more significant change in potential after the shoulder. These results can easily be reconciled with the impedance diagram given in Fig. 2a of Part I [1]. The instantaneous voltage drop in Fig. $6a_1$ of 100 mV correlates directly with the high frequency intercept given in Fig. 2a of Part I of

50 mΩ on the basis of Ohm's law for a 2-A current, i.e. $\Delta V = 2R$. Similarly, the voltage drop over the region of the shoulder in Fig. $6a_1$ of ~ 50 mV correlates approximately with the diameter of the semicircle in Fig. 2a of Part I of 20 mΩ. Furthermore, the initial voltage drop in Fig. $6a_2$ of 150 mV correlates satisfactorily with the low frequency intercept of the semicircle given in Fig. 2a of Part I of 70 mΩ. These results demonstrate clearly the need to observe the pulse profile over a contracted time scale in order to extract the maximum information and avoid the situation in Fig. $6a_2$ where only the sum of the various ohmic potential drops is discernible as $t \rightarrow 0$. At longer times, as exemplified by the pulse tail in Fig. $6a_2$, Ohm's law cannot be used to correlate the pulse and impedance behaviour because concentration polarization within the MnO_2 particles occurs. Nevertheless, it is obvious that this region after the shoulder corresponds to the low-frequency linear impedance region given in Fig. 2a of Part I [1].

The Ohm's law correlations discussed above indicate that over the region of the instantaneous potential drop and the shoulder of Fig. $6a_1$, the equivalent circuit is represented by the left hand side of Fig. 4 including the first two R–C networks. This is identical to the situation pertaining in short-circuit current measurements. An inspection of the other pulse characteristics shown in Fig. 6b–e shows a similar correlation with the remaining correspondence spectra given in Fig. 2b–e of Part I, respectively. Thus the potential response of the cathode current collector shown in Fig. $6c_2$ is an almost perfect 85 mV square wave which correlates exactly with the 42 mΩ low frequency intercept on the impedance diagram in Fig. 2c of Part I. Similarly, the potential response of the anode–separator system shown in Fig. $6e_2$ is a square wave of amplitude 45 mV which correlates exactly with the 23 mΩ impedance intercept in Fig. 2e of Part I, which can be attributed predominantly to electrolyte resistance within the anode and separator matrices. The absence of any subsequent fall in potential after the initial instantaneous drop due to the very small polarization at the zinc electrode is evidenced by the extremely low impedance value attributable to the zinc electrode reaction even at the lowest frequencies (see Fig. 2e of Part I [1]).

Having established a working basis for comparing the initial pulse discharge and impedance characteristics, it was of interest to deliberately affect a change in the internal cell resistance and observe whether the above correlations continued to be obeyed. A breakdown of the impedance characteristics for a non-standard LR20 alkaline manganese cell (constructed using a cathode can which had been heated in air at 600°C to produce a thicker oxide layer on the nickel-plated steel surface than normal is shown in Fig. 4 of Part I [1]. Again, a detailed interpretation of the impedance spectra has been given previously [1]. Essentially, the only difference between the spectra in Figs 2 and 4 of Part I is that the size of the semicircle is considerably increased. Therefore the main difference between the pulse characteristics expected for the standard and non-standard cells would be an increase in the voltage drop over the region of the shoulder in the case of the 10 ms pulse (contracted time scale) and an increase in the initial voltage drop in the case of the 4 s pulse (expanded time scale). Fig. 7 confirms these predictions. In the case of the pulse characteristics for the whole cell (Fig. 7a) the instantaneous potential drop is 90 mV which correlates exactly with the high frequency intercept of 45 mΩ in Fig. 4a of Part I. This is almost identical to the high frequency intercept for the standard cell of 50 mΩ (cf. Fig. 2a of Part I). The voltage drop over the shoulder in Fig. $7a_1$ is 350 mV, which correlates exactly with the diameter of the semicircle of 175 mΩ in Fig. 4a of Part I. This is almost nine times greater than the value for the standard cell of 20 mΩ (cf. Fig. 2a of Part I). Moreover, since the nickel oxide has capacative as well as resistive properties, the greater time elapsed over the region of the shoulder in the case of the non-standard cell indicates a slower rate of oxide charging. This can also be seen in the impedance diagrams from a comparison of the relaxation times $= 1/(2\pi f^*)$ where f^* is the critical frequency at the top of the semicircles (cf. Figs 2 and 4 of Part I). Finally, the voltage drop at longer times, which correlates with the Warburg impedance due to concentration polarization, is again very similar

Table 1. Comparison of measured potential drops in mV across individual LR20 cell components obtained from short-time 2-A pulse discharge measurements with those calculated from impedance spectra determined at the open-circuit potential

Technique	*Whole cell*		*Cathode + can*		*Can*		*Cathode*		*Anode + separator*	
	$t \to 0$ *or* $\omega \to \infty$	$t = 10\,ms$ *or* $\omega \to LFI$	$t \to 0$ *or* $\omega \to \infty$	$t = 10\,ms$ *or* $\omega \to LFI$	$t \to 0$ *or* $\omega \to \infty$	$t = 10\,ms$ *or* $\omega \to LFI$	$t \to 0$ *or* $\omega \to \infty$	$t = 10\,ms$ *or* $\omega \to LFI$	$t \to 0$ *or* $\omega \to HFI$	$t = 10\,ms$
Pulse*	100	150	80	150	30	85	50	65	45	45
Impedance*	100	140	64	136	40	84	52	52	46	46
Pulse†	90	460	100	450	10	340	90	110	40	40
Impedance†	90	448	100	480	5	376	95	104	54	54

* Standard cell; † non-standard cell.
LFI = Low frequency intercept; HFI = high frequency intercept.

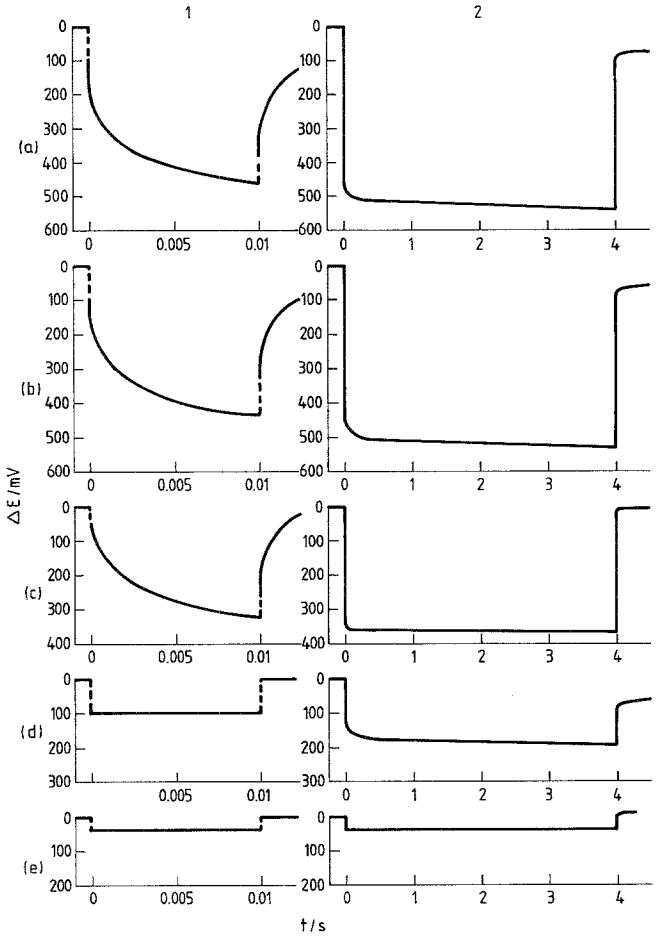

Fig. 7. Galvanostatic 2-A pulse discharge characteristics taken over 10 ms (column 1) and 4 s (column 2) for various components in a non-standard LR20 alkaline manganese cell. The component designations are identical to those described in Fig. 6.

to that for the standard cell (cf. Figs $6a_2$ and $7a_2$).

Table 1 summarizes the pulse and impedance data in respect of the whole cell and individual cell components. The data for the cathode alone has been determined by subtracting that for the can (reference electrode position 2) from that for the cathode–can assembly (reference electrode position 1) as discused in [1]. It must be emphasized, however, that the act of inserting reference electrodes into the cells must have a disturbing effect upon the cell components which is also somewhat variable from one situation to another. Therefore the sum of the pertinent impedance or pulse parameters for individual cell components does not necessarily agree exactly with those for the complete cell. Electrolyte redistribution may be partly responsible.

The above results fully vindicate the electrical analogue circuit presented in Fig. 4 and demonstrate the equivalence of the initial pulse discharge behaviour and impedance characteristics. However, a further important deduction is possible. It can be estimated from Fig. $6a_2$ that the magnitude of the voltage drop due to polarization of the MnO_2 electrode is typically about 100 mV for a standard cell over the time scale of a 10 s galvanostatic 2-A pulse. Since the total potential drop across the cell approaches 300 mV, 67% of the voltage loss can be attributed to internal cell resistance. This figure would, of course, be very much higher for cells having a greater internal resistance than the standard value. As a result of these conclusions it can be deduced that in the case of a typical repetitive 2 A/10 s pulse discharge regime, the discharge life will be critically dependent upon the internal resistance value.

5. Conclusions

1. A proper interpretation of the short-circuit current behaviour of primary cells requires a detailed knowledge of the equivalent circuit for the cell system concerned. From the equivalent circuit the pertinent internal resistance value for the cell can be specified and correlated with short-circuit current value. The internal resistance is a composite of several components.

2. In the case of alkaline manganese cells, three resistances predominantly determine the internal resistance value. These can be independently resolved using *in situ* impedance measurements because two of them are associated with parallel capacitive components in the equivalent circuit. They are: the electrolyte resistance within the anode–separator–cathode porous matrices; the resistance of the cathode (MnO_2 + graphite mixture); and the resistance of the nickel oxide layer on the surface of the nickel-plated steel positive current collector.

3. In the case of Leclanché cells three resistances also control the internal resistance value, but these cannot be so easily resolved because no parallel capacitive components can be detected when the impedance of the *whole* cell is measured. They are: the electrolyte resistance within the cathode–separator matrices; the resistance of the cathode (MnO_2 + carbon mixture); and contact resistance between the cathode and positive current collector (carbon rod).

4. Short-time (10 ms) galvanostic 2-A pulse measurements can be correlated directly with impedance measurements thus providing confirmatory evidence for the equivalent circuit. In the case of standard LR20 cells the resistance calculated from the potential drop at 10 ms correlates almost exactly with the internal resistance and hence the short-circuit current value.

5. Long-time (10 s) galvanostatic 2-A pulse measurements on standard LR20 cells indicate that ohmic polarization constitutes 67% of the total potential loss. It can therefore be deduced that in the case of a typical repetitive 2 A/10 s pulse discharge regime, the discharge capacity will be critically dependent upon the cell internal resistance value.

Acknowledgements

The authors would like to thank Dr N. C. White for the data in Fig. 2 and the Directors of British Ever Ready Limited for permission to publish this work.

References

[1] R. Barnard, L. M. Baugh and C. F. Randell, *J. Appl. Electrochem.* **17** (1987) 165.

[2] R. J. Brodd and H. J. De Wane, *J. Electrochem. Soc.* **110** (1963) 1091.

[3] W. J. Hamer, in 'The Primary Battery', Volume II, (edited by N. C. Cahoon and G. W. Heise) John Wiley and Sons, New York (1976) Chap. 10, p. 429.

[4] L. M. Baugh and N. C. White, paper presented at the 15th International Power Sources Symposium, Brighton, UK, September 1986, and to be published in 'Power Sources 11', (edited by L. Pearce).

[5] S. A. G. R. Karunathilaka, N. A. Hampson, R. Leek and T. J. Sinclair, *J. Appl. Electrochem.* **10** (1980) 357.

[6] S. Atlung and T. Jacobsen, *Electrochim. Acta.* **21** (1976) 575.